Spatially Resolved High Voltage Kelvin Probe Force Microscopy: A Novel Avenue for Examining Electrical Phenomena at Nanoscale

RESEARCH ARTICLE

ADVANCED PHYSICS RESEARCH Open Access

www.advphysicsres.com

Spatially Resolved High Voltage Kelvin Probe Force Microscopy: A Novel Avenue for Examining Electrical Phenomena at Nanoscale

*Conor J. McCluskey, Niyorjyoti Sharma, Jesi R. Maguire, Serene Pauly, Andrew Rogers, TJ Lindsay, Kristina M. Holsgrove, Brian J. Rodriguez, Navneet Soin, John Marty Gregg, Raymond G. P. McQuaid, and Amit Kumar**

Kelvin probe force microscopy (KPFM) is a well-established scanning probe technique, used to measure surface potential accurately; it has found extensive use in the study of a range of materials phenomena. In its conventional form, KPFM frustratingly precludes imaging samples or scenarios where large surface potential or surface potential gradients exist outside the typical ±10 V window. If the potential regime measurable via KPFM can be expanded, to enable precise and reliable metrology, through a high voltage KPFM (HV-KPFM) adaptation, it can open up pathways toward a range of novel experiments, where the detection limit of regular KPFM has so far prevented the use of the technique. In this work, HV-KPFM is realized and shown to be capable of measuring large surface potential and potential gradients with accuracy and precision. The technique is employed to study a range of materials (positive temperature coefficient of resistivity ceramics, charge storage fluoropolymers, and pyroelectrics) where accurate, spatially resolved mapping of surface potential within high voltage regime facilitates novel physical insight. The results demonstrate that HV-KPFM can be used as an effective tool to fill in existing gaps in surface potential measurements while also opening routes for novel studies in materials physics.

1. Introduction

Kelvin probe force microscopy is a scanning probe technique that allows quantitative, spatially resolved mapping of the Contact Potential Difference (CPD) or the surface potential on the nanoscale.[1] For metals and semiconductors, the measured surface potential is reflective of the local work function differences between the tip and the sample,[2] but, in the case of insulators, the primary contributions to the potential come from the presence of uncompensated surface charges.[3] KPFM and its adaptations (examples being time-resolved KPFM[4] and contact-mode KPFM[5]) continue to be heavily used scanning probe techniques for the study of a range of physical phenomena in functional oxides and 2D materials.[6–9] KPFM is particularly useful in studying ferroelectrics, where changes in surface charge species and densities can provide insight into the static or dynamic properties of the bulk polarized domains.[10–13]

Frustratingly, many current implementations of the KPFM technique preclude imaging large surface potentials exceeding ±10 V or in scenarios in which large surface potential gradients exist. This constraint likely arises from the technique's historical emphasis on measuring the work function in metals and semiconductors, where differences exceeding ±10 V

C. J. McCluskey, N. Sharma, J. R. Maguire, S. Pauly, A. Rogers, T. Lindsay, K. M. Holsgrove, J. M. Gregg, R. G. P. McQuaid, A. Kumar
Centre for Quantum Materials and Technologies
School of Mathematics and Physics
Queen's University Belfast
Belfast BT7 1NN, UK
E-mail: a.kumar@qub.ac.uk

The ORCID identification number(s) for the author(s) of this article can be found under https://doi.org/10.1002/apxr.202400011

DOI: 10.1002/apxr.202400011

B. J. Rodriguez
School of Physics
University College Dublin
Belfield, Dublin 4, Ireland

N. Soin
School of Engineering
Ulster University
2–24 York Street, Belfast BT15 1AP, UK

N. Soin
School of Science
Computing and Engineering Technologies
Swinburne University of Technology
P.O. Box 218, Hawthorn, VIC 3122, Australia

are improbable, given that the reported work function values for elements range from ≈2 to 6 eV. Nevertheless, the extension of KPFM into the high voltage (HV) regime (HV-KPFM) presents an intriguing avenue for uncovering deeper insights into material behavior, particularly within the context of dielectrics and ferroelectrics. These materials can give rise to substantial surface potentials, on the order of hundreds to thousands of volts in bulk crystals and films and such high potentials can lead to novel functionalities. Regrettably, conventional KPFM falls well short in measuring such potentials effectively due to its inherent limitations.

In the context of ferroelectrics and dielectrics, many interesting problems and opportunities have emerged recently where spatially resolved HV-KPFM can provide clinching experimental evidence to help unveil new physical insights. Two clear examples are 4-probe characterization of conducting domain walls[10] and quantitative Hall voltage mapping[11] in situations where the lateral driving voltage across walls is larger than the typical range achievable through KPFM. In triboelectric dielectrics, large voltages can develop during the charging and contact-electrification processes and HV-KPFM can offer insight through direct visualization of the spatial distribution of such charging–discharging processes. HV-KPFM also could offer a viable platform for studying the surface potential development in pyroelectric crystals for small temperature changes, which is not possible using conventional KPFM (pyroelectric potentials can easily exceed tens of volts for a small change in temperature). Despite the opportunity for HV-KPFM for materials explorations, literature shows a striking dearth of attempts to make a working HV-KPFM system.

There have been some efforts, using external feedback loops, HV sources, and Arduino-based software. These endeavors have primarily focused on examining line profiles of surface potentials along the channels of organic thin-film transistors.[14] The addition of external feedback loops, however, can often give rise to electronic offsets at the AFM controller inputs/outputs and electronic cross talk and therefore requires a rigorous design and troubleshooting methodology to remove any offset-induced artefacts. A feedback-free HV modality (KPFM-HV) is also available on certain commercial AFM systems, which does not rely on the use of a HV source. Instead, it utilizes an oscillating AC voltage applied to the probe and calculates the electrostatic potential by measuring the cantilever response at the first- and second harmonics.[15] This process necessitates driving the cantilever significantly away from its mechanical resonance frequency, to avoid harmonic coupling and cantilever-crosstalk issues. In this case, the CPD is calculated using the amplitudes of first- and second-harmonics simultaneously captured *via* two separate lock-in amplifiers thus increasing the system complexity. The lack of a fully developed High-Voltage KPFM, offered on standard AFMs, may also stem historically from clear identification of problems where such measurements could help reveal new phenomena or enable new physical insight. The conspicuous absence of HV-KPFM as a standard operational mode thus underscores a potentially significant gap in our understanding of material behavior at elevated surface potentials and raises questions about the extent to that HV-KPFM has been underutilized in scientific research.

In this work, we have extended the KPFM voltage regime on a commercial atomic force microscope to ±150 V. First, we demonstrate proof of principle experiments under known, controlled conditions: we show that our HV-KPFM technique can accurately measure the surface potential applied to a metallic pad and use the technique to track surface potential profiles in the high voltage regime, by independently measuring the potential difference across an inter-electrode gap where a large (50 V) applied voltage decays to ground within a single scan window. Then, we show that our technique is applicable to real material characterization problems, by extending recent experiments from literature to the high voltage regime. Specifically, we track the surface potential build-up and charge neutralization in Polytetrafluoroethylene (PTFE) films when bombarded by ionic charges, and we spatially map the potential barriers across grain boundaries in positive temperature coefficient of resistivity (PTCR) ceramics. Finally, we introduce and demonstrate a novel, HV-KPFM based approach for the measurement of pyroelectric coefficients in bulk single crystals, by measuring the voltages developed on the terminating surfaces of pyroelectric materials upon heating and cooling. The results clearly demonstrate that HV-KPFM can be used as a novel and effective tool to fill in existing gaps in surface potential and potential gradient measurements, while also opening pathways for novel studies in materials physics.

1.1. Methodology

In KPFM, a metallic AFM tip makes two consecutive passes over the sample surface. The first is a traditional tapping mode topography measurement, where the tip is mechanically oscillated as it moves across the surface. Changes in topography are counteracted (and therefore inferred) by a feedback mechanism, which extends or retracts the tip to keep the oscillatory motion constant. In the second pass, the tip retraces the sample topography, this time at a constant, user-defined lift height, meaning the tip-sample distance remains constant, even over rough topography. An AC electrical bias is applied to the tip, with a frequency close to its mechanical resonance frequency, to induce oscillatory motion via capacitive forces between the tip and the sample. The first harmonic of this oscillatory force depends on the D.C. potential difference between the tip and sample, so by supplying an additional offset D.C. voltage to the tip (V_{DC}, which is equal to the tip-sample potential difference), the oscillation is nullified. In this case, the oscillation of the tip, at the frequency of the applied AC bias, and acts as the feedback signal for the applied DC bias. The map of the nullifying DC bias across the surface is a direct image of the true surface potential. Importantly, the magnitude of the voltage limit of the hardware of most off-the-shelf AFMs is 10 V. As KPFM can only measure what can be applied to the AFM tip, so this becomes the de facto measurement limit.

Here, we have employed a high voltage (HV) module, customized for the MFP-3D Infinity system, around which the HV-KPFM experiment is designed. A customized isolated stage (Figure S1, Supporting Information) is used in the experiment that carries the high voltage generated using a high voltage amplifier integrated on to a relay enabled card that then communicates directly to the Asylum Research Controller (ARC). The HV tip holder (Figure S1, Supporting Information) is also custom

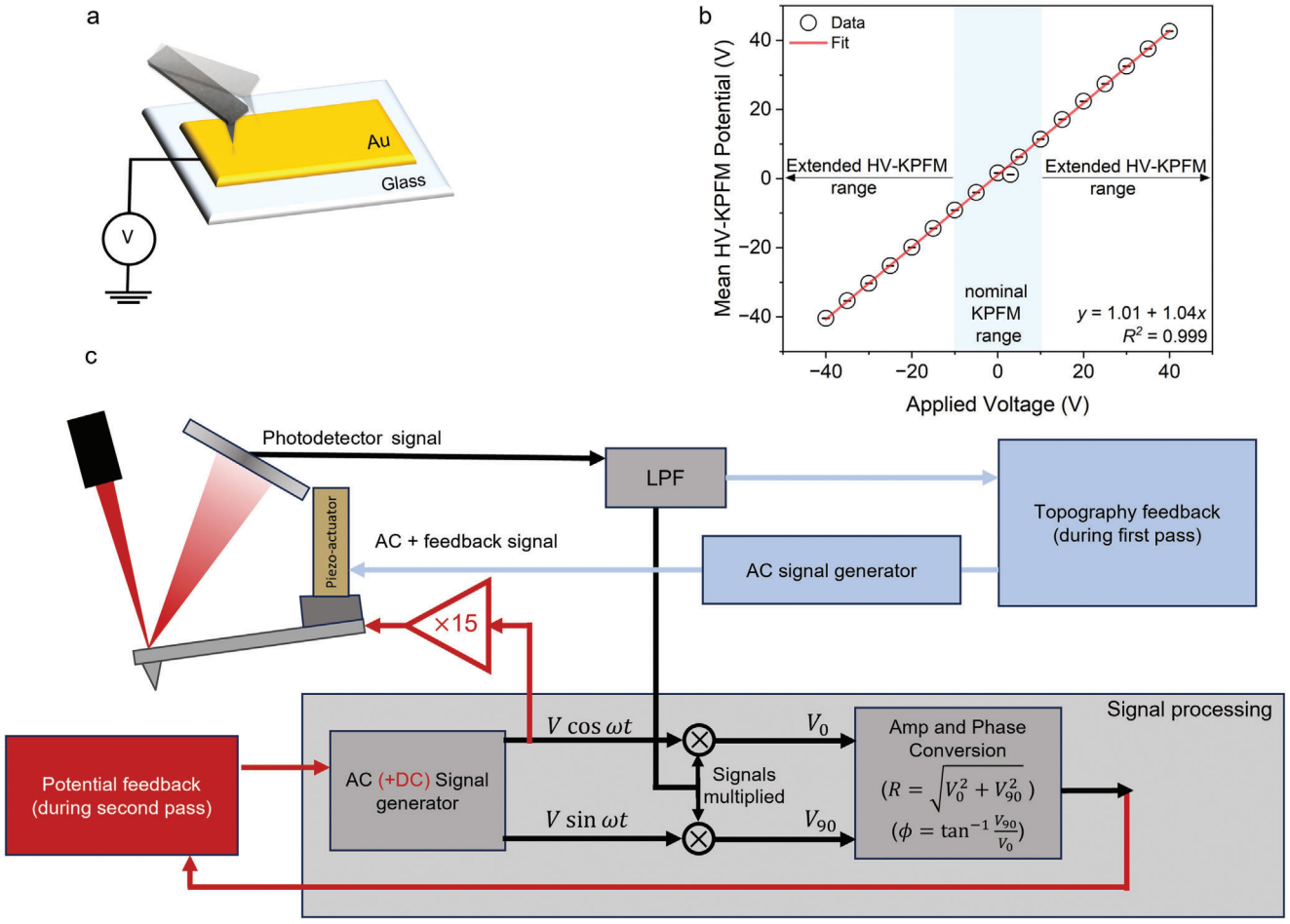

Figure 1. An illustration of surface potential measurement in the high voltage regime. a) The measurement is undertaken on a single spot on the gold electrode that has bias applied via a bias source b) Measured surface potential using HV-KPFM setup shows excellent agreement with the applied voltage. c) Schematic illustrating the HV-KPFM implementation on the Asylum Research MFP Infinity system where a 15x amplifier circuit is employed during the second pass (adapted from the Asylum Research MFP-3D Infinity AFM manual).

designed, such that the bias supplied to the HV stage is directly routed to the metallic tip, which in turn is fully isolated from the electronics that mechanically drive the tip (thus enabling KPFM). This isolation of the high voltage to the tip is crucial in protecting the remaining circuitry of the AFM head and is illustrated in **Figure 1**. The HV module generates precise AC+DC signals between −150 and +150 V with no significant delays meaning HV-KPFM can be performed at speeds comparable to conventional KPFM. The advantage that this approach has, over alternative methods, is that the AFM controller communicates directly with both the piezo control and the high voltage module (that supplies DC voltage to the tip), making the feedback loop more efficient and reliable than introducing external electronics and feedback loops. During scanning in the interleave pass, the appropriate mix of AC and DC voltages is directly routed to the tip through the AFM software. The software control panel has been customized, such that the nullifying voltage can be directly recorded at each pixel in a precise manner. As a result, precise measurements of the surface potential could then be made possible on the nanometer scale therefore enabling spatially resolved HV-KPFM.

2. Results and Discussion

2.1. Proof-of-Concept

A simple proof-of-concept experiment demonstrating HV-KPFM is shown in Figure 1. A DC voltage, supplied by an external power supply unit, was supplied to a planar gold electrode that was sputtered onto a glass slide. A standard Pt-Ir coated AFM tip was then brought into contact with the electrode and HV-KPFM was performed at a single spot on it (a "point scan", as illustrated in Figure 1a). The bias supplied to the electrode ranged between −40 and 40 V, which is accurately mapped by the measured HV-KPFM potential (Figure 1b). The data points and errors in Figure 1b are taken as the mean and standard deviation from 256 × 256 KPFM data points, all taken at the same x-y position on the electrode. Errors from the mean value are on the order of ±0.06 V, which include errors from crosstalk with the topography signal.[16,17] It is suspected that this crosstalk contributes to the majority of the error.

HV-KPFM has the capability not only to measure large surface potentials, but to accurately resolve the spatial profile of

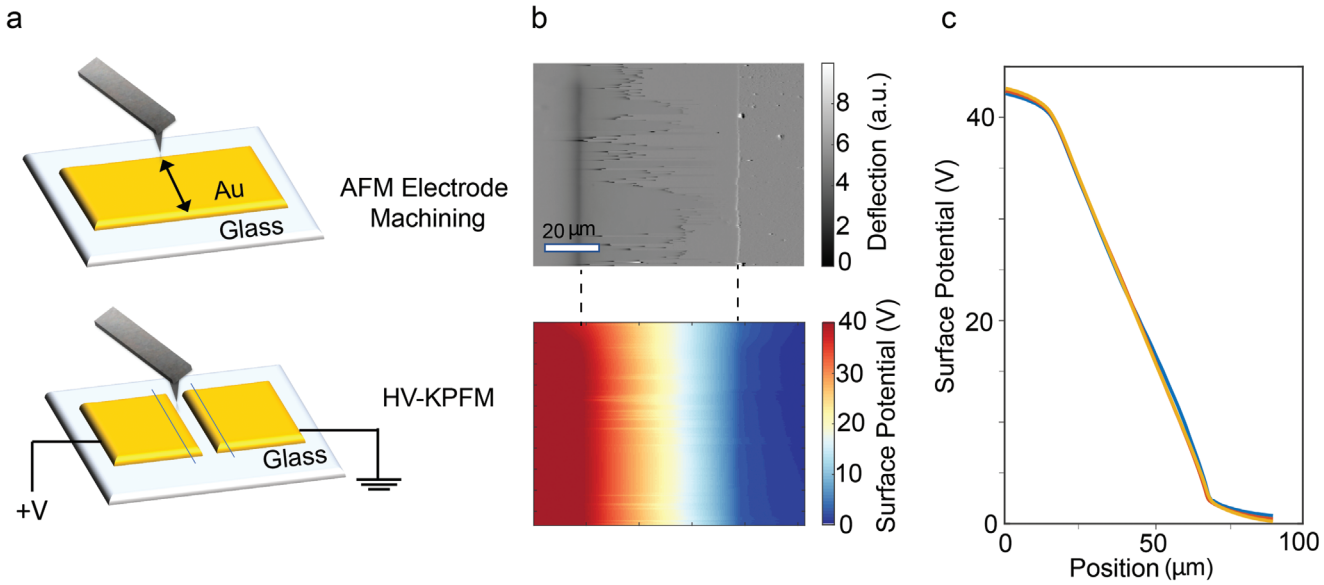

Figure 2. HV-KPFM based potential gradient mapping a) Schematic illustrating AFM based milling to create an interelectrode gap when potential gradient is mapped b) HV-KPFM potential map of the region indicated in a) showing steep drop of the applied potential across the electrodes c) Three line profiles of the potential drop across the gap are observed to be linear in line with expectations.

large surface potentials with nanoscale resolution. To show this, a gold bar was sputtered, again onto a glass slide, and an interelectrode gap was AFM machined into the bar, using established AFM tip-based machining techniques.[18,19] A large potential difference was then applied between the two now-separated electrodes. The process is schematically represented in **Figure 2**a. Figure 2b shows a HV-KPFM surface potential map of the interelectrode region. The map shows clearly a relatively flat potential profile of ≈40 V (0 V) measured on the high (low) electrode, and a linear potential drop across the interelectrode gap. Figure 2c plots three line sections taken across the interelectrode gap. The values match those that we might expect for the externally applied voltage of 40 V. This experiment validates that HV-KPFM has the ability to map potential profiles in the high voltage with the same high spatial resolution as typically afforded by conventional atomic force microscopy techniques. In principle, this neatly extends the range of physical phenomena that can be examined with surface potential mapping by KPFM.

2.2. Grain Boundary Potential Mapping in PTCR Ceramic

The ability to precisely map surface potentials in lateral geometries where bias is applied across electrodes brings out interesting possibilities in terms of exploring transport in materials. Typically, when a lateral electric field is applied to a material with homogeneous electrical properties, the change in potential is linear (as seen in Figure 2c). However, deviations from linearity in the potential profile can be used to evaluate the role of microstructural inhomogeneity in electrical transport[20] as well as determination of electronic transport characteristics in the presence of magnetic fields. An example of the latter application is a KPFM based Hall-potential detection technique utilized to investigate the carrier transport at charged conducting ferroelectric domain walls.[11,21] In addition, the spatial distribution of electric potential dropped along curved current-carrying conducting domain walls in classic insulators such as $LiNbO_3$ can be mapped using KPFM in the high voltage regime and such efforts can even unveil physics associated with ferroelectric domain wall p-n junctions (otherwise very difficult to characterize).[22] Moreover, HV-KPFM could in principle allow the visualization of more extreme electronic transport regimes (such as ballistic transport), which become evident only under high electric fields, involving potential drops beyond the limits of conventional KPFM.

In prior work undertaken by our team, conventional KPFM was used to investigate the role of grain boundaries in a PTCR ceramic in a lateral geometry where they form part of the electrical circuit.[20] It was shown that, even in the low-resistance ferroelectric state, the potential drop at grain boundaries is significantly greater than in the grain interiors. Due to limitations of examinable bias range in KPFM, it was not possible to map the entire interelectrode gap in such measurements as significant field drop occurred at electrodes. Here, we have employed HV-KPFM to evaluate the entire field profile across the interelectrode gap on polished PTCR ceramic with up to 40 V applied in lateral geometry. Our goal was also to accentuate the non-linear change in the field associated with the grain boundaries and how it evolves as the applied bias is increased. **Figure 3**a shows a topography map of a polished region on the PTCR ceramic with the corresponding grain boundaries outlined in Figure 3b. The spatial profile of the potential and its derivative are shown in Figure 3c,d respectively. It is worth noting that a significant fraction of the applied bias is dropped at the right-hand electrode/ceramic junction, as evidenced by the concentration of the field in Figure 3d. Beyond this junction, the voltage drop across the gap has a more linear trend and the potential derivative map shows enhanced drops at the grain boundaries, a result that confirms that these interfaces are indeed much more resistive than the bulk (interior) of the

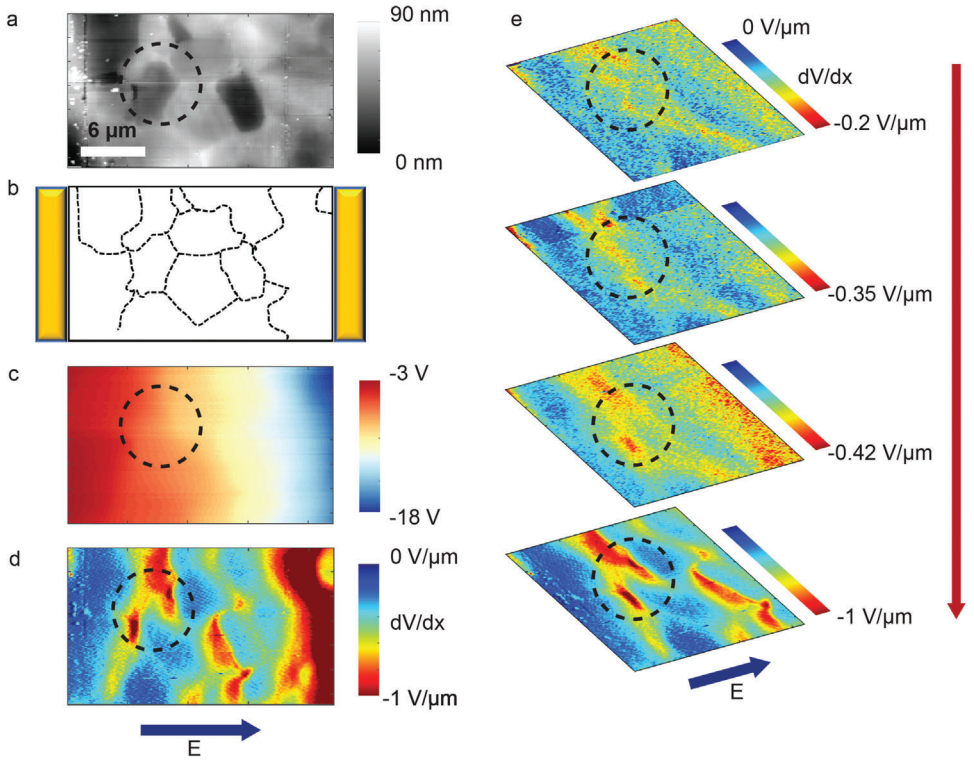

Figure 3. Mapping grain-boundary mediated electrical transport in PTCR ceramics. a) Topography of the BTO-PTO-CTO surface for the KPFM experiment (26 × 13 μm), with Au electrodes placed parallel to the scan direction. b) Schematic of the scanned area, c) Potential map acquired by applying −20 V across the surface of the sample, measured using HV-KPFM and d) gradient of the potential map. The concentration of electric field on one electrode illustrates that a significant fraction of the applied voltage drops at the electrode-ceramic junction. e)Potential gradient maps with increasing electric field mapped via HV-KPFM demonstrate the key role of grain boundaries in determining electrical transport in the PTCR ceramic.

grain. A trimmed section of the derivative maps obtained, at increasing biases, shows that the potential drop (and hence the local field) increases at the grain boundaries. It is worth pointing out that the gradient maps look qualitatively different at higher biases with large potential drops more concentrated near the grain boundaries. Thus, HV-KPFM enables us to measure the changes in potentials at grain boundaries more vividly and further reinforce their role in mediating the conduction in PTCR ceramics (in congruence with the Heywang–Jonker model).[23]

2.3. Assessing Static Charge-Induced Surface Potential in Insulators

The HV-KPFM technique can also be extended to study charging dynamics in materials in regimes beyond ±10 V. Typically, highly crystalline fluoropolymers, such as PTFE, fluorinated ethylene propylene, and polyvinylidene fluoride, exhibit the highest electron affinities thus leading to remarkably large surface potentials.[24] As such, utilizing electret, piezoelectric, and triboelectric phenomena, these materials form the backbone of energy harvesting platforms.[25] Particularly, tribo-negative PTFE is the material of choice for sliding- and contact- mode nanogenerators, wherein nano-structuring or corona-discharge processes are undertaken to enhance its macroscopic exchange charge density.[26,27] However, the nanoscale imaging of the induced changes is limited to either qualitative electrostatic force microscopy or the restricted conventional KPFM imaging, neither of which allows quantitative nanoscale spatial evaluation of the surface potential. We have assessed the applicability of HV-KPFM to study the surface potential values for as-obtained PTFE but to also track and quantify charge injection (and neutralization) processes. For thin PTFE films (12.7 μm) the typical laminar arrangement of the globular structures visible in the topography (left column of **Figure** 4b, upper row) is not reflected in the potential map owing to channel saturation (left column of Figure 4b, lower row). In comparison, HV-KPFM taken from a slightly different adjacent area (see right column of Figure 4b, lower row) was able to successfully map and quantify this surface potential in the range of −34 to −40 V, whose origins lie in the stretching induced orientational effects and resultant charge trapping characteristics. The control experiment in Figure 2 suggests that cross talk is not a particularly pertinent issue in HV-KPFM, so the topography-like features represented in the HV-KPFM map show genuine potential changes across the sample surface. To replicate the effects of nano-structuring/high-voltage induced enhanced charge density, we utilize a charge injection process with controlled polarizability. Figure 4c–e shows the HV-KPFM surface potential maps of the PTFE sample at different stages of the charge injection process. First, the surface was neutralized (using positive charges) consequently lowering the surface potential to ≈−9.4 V. The subsequent negative charge injection cycles significantly increased the surface potential value in the negative regime to ≈−119.9 V. Last, positive charges were injected, to raise the surface potential

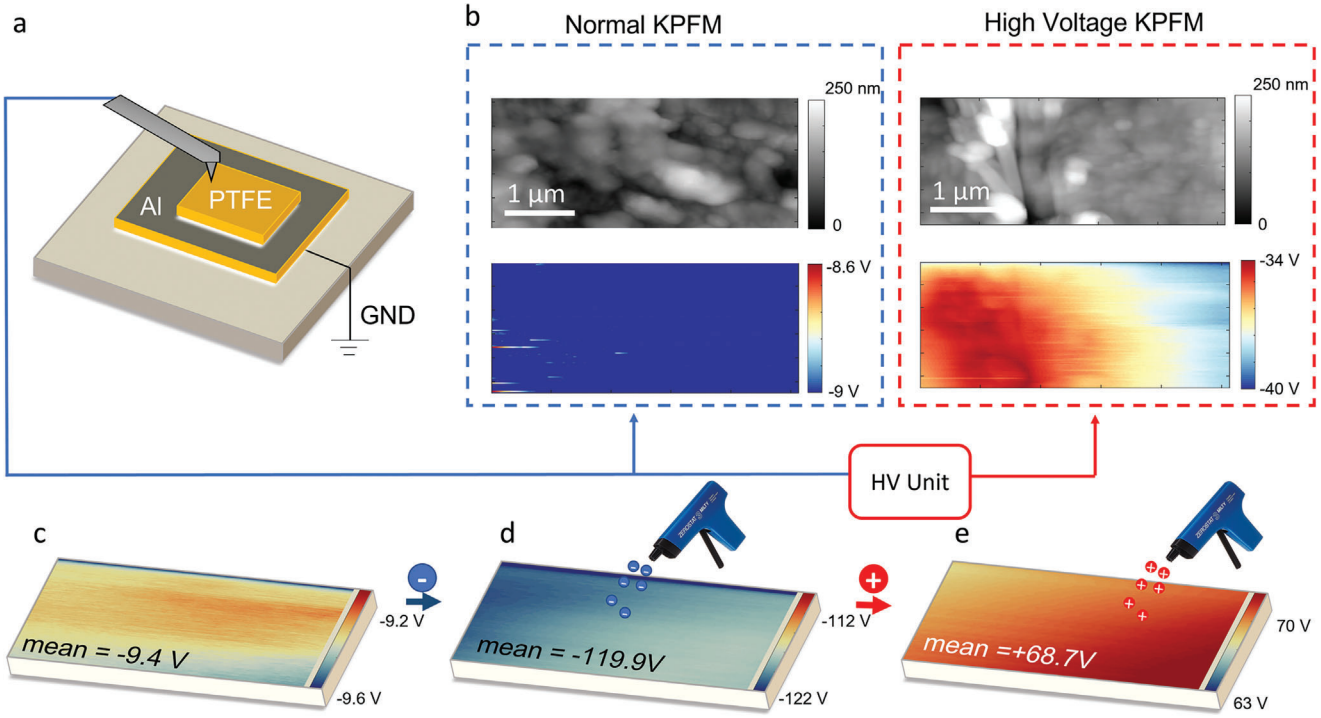

Figure 4. Evaluating charge injection in polymer films using HV-KPFM. a) Schematic of spatially resolved HV-KPFM on Polytetrafluoroethylene (PTFE) film b) Topography and conventional KPFM potential map that is saturated and unable to measure the true surface potential in this film compared with HV-KPFM data that shows correlation of surface potential with microstructure in −34 to −40 V regime c) spatially resolved HV-KPFM potential maps of the film upon charge neutralisation (using positive charges) d) negative charge injection and e)positive charge injection with a charge gun illustrate the effective surface potential mapping on the nanoscale in this material.

to a value of +68.7 V. These charge states arose from the presence of trapped, uncompensated charges on the surface, and could easily be manipulated, and monitored, as shown here.[28] The associated charge densities could be harnessed to make more efficient triboelectric nanogenerator devices with still higher voltage outputs.

2.4. HV-KPFM Assessment of Pyroelectric Coefficient of Ferroelectrics

The presented results illustrate the direct implications of HV-KPFM for evaluating material physics via quantitative measurement of surface potentials in the high voltage regime. The developed technique can also open up new ways of measuring material properties linked to surface potential, where conventional KPFM simply could not be used. In this context, we have employed HV-KPFM to measure pyroelectric coefficients of ferroelectric crystals. Pyroelectric materials exhibit a change in the spontaneous polarization vector in response to temperature changes.[29] This results in a change in the bound surface charge on the terminating crystal surfaces normal to the polarization. Typically, pyroelectric behavior in ferroelectrics is measured by measuring the voltage across a reference capacitor or by measuring the pyroelectric current through a reference resistor, upon changes in temperature. Undertaking this measurement on the nanoscale requires a metallic tip to be able to accurately read the potential on the surface. Prior attempts to employ KPFM in measuring pyroelectric behavior in ferroelectrics have been limited to thin films[30] due to the possibility of large potential build-up in single crystals for small changes in temperatures.

The 'true' pyroelectric coefficient of a material can be expressed (under constant stress) as shown in Equation (1),

$$p = \left(\frac{\partial P}{\partial T}\right)_{s,i} = \left(\frac{\partial P}{\partial E}\right)_{s,i} \times \left(\frac{\partial E}{\partial T}\right) \quad (1)$$

where p refers to the true pyroelectric coefficient, P refers to spontaneous polarization, T indicates temperature, and E refers to the electric field. It is worth noting that this value is different from the 'generalized' pyroelectric coefficient that relates dielectric displacement to changes in temperature. For a monodomain ferroelectric crystal of thickness d, this expression further reduces (with suitable assumptions) to that shown in Equation (2).

$$p = \epsilon_0 \epsilon_r \frac{\Delta V}{d\Delta T} \quad (2)$$

Thus, the change in surface potential ΔV arising from a temperature change of ΔT is given as follows:

$$\Delta V = \frac{p\Delta T\, d}{\epsilon_0 \epsilon_r} \quad (3)$$

where ϵ_r is the dielectric constant and ϵ_0 indicates the permittivity of vacuum. An important assumption made to arrive at Equation (3) is that the chosen permittivity value assumes a linear

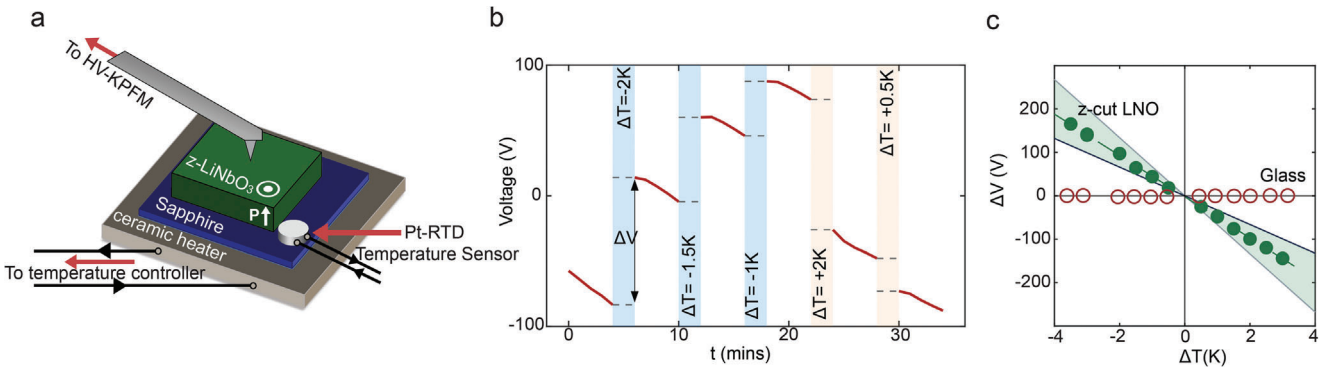

Figure 5. Measurement of pyroelectric coefficient in a ferroelectric single crystal of $LiNbO_3$ via HV-KPFM. a) Schematic illustrating a z-cut $LiNbO_3$ crystal on a temperature controlled ceramic heater with HV-KPFM used to measure changes in surface potential quantitatively after each temperature step (ΔT) b) The change in voltage ΔV after each temperature step is measured c) Plot of ΔV vs ΔT gives pyroelectric coefficient of −63 μC m^{-2} K that lies between range of values reported for $LiNbO_3$ crystals (−41 to −83 μC m^{-2} K).[31–34] A reference sample of glass shows no pyroelectric behavior in line with expectations.

dielectric behavior regime for the examined sample. Reported pyroelectric coefficients for single crystal $LiNbO_3$ (along the polar [001] axis) lie between −41 and −83 μC $(m^2\ K)^{-1}$.[31–34] This means that for a 175 μm thick z-cut crystal, a potential difference of 19 to 37 V should be expected for just 1 K change in temperature on the [001] face, rendering conventional KPFM ineffective (as the surface potential scales with crystal thickness, potentials of up to 3 kV can be observed for a 10 mm crystal of LNO for just 1 K change in temperature). Hence, HV-KPFM offers an ideal nanoscale platform to measure pyroelectric coefficients in ferroelectric crystals, and furthermore, offers the functionality to measure spatial variations in pyroelectric properties.

The setup for measurement of pyroelectric coefficients in a ferroelectric single crystal of $LiNbO_3$ via HV-KPFM is illustrated in **Figure 5**a. A z-cut monodomain $LiNbO_3$ crystal is polished to a thickness of 175 μm and placed on a sapphire crystal that in turn sits on a ceramic heater, whose temperature can be accurately controlled (to within ≈0.1 K) and measured via a temperature sensor. With each temperature step, the change in surface potential is measured. As shown in Figure 5b,c, change in voltage is linear with the change in temperature and reveals a pyroelectric coefficient of −63 μC $(m^2K)^{-1}$. This observed value sits in the middle of reported values for pyroelectric coefficient of $LiNbO_3$ indicated by the shaded region shown in Figure 5c. Similar studies were undertaken on $LiTaO_3$ crystals (higher pyroelectric coefficients, see Table S1, Supporting Information) as well as amorphous glass substrates (no response, see Table S2, Supporting Information) and results were found to be consistent with expectations (see section 2 in Supp. Mater.). In essence, HV-KPFM offers a unique approach to measure pyroelectric coefficients in single crystal ferroelectrics and could, in principle, enable nanoscale spatially resolved mapping of pyroelectric behavior in ferroelectric crystals with complex microstructures.

3. Conclusion

In conclusion, we have introduced and investigated a high-voltage Kelvin probe force microscopy technique, capable of reliably measuring surface potentials well beyond the conventional ±10 V limit. We have demonstrated the accuracy of the technique, by mapping known potential profiles across interelectrode gaps, in excess of 10 V. We have also applied HV-KPFM to real material characterization problems; we map the charging and discharging in PTFE (a material key for triboelectric voltage generation), and we image the functional response of grain boundaries in positive temperature coefficient of resistivity (PTCR), all in a voltage regime inaccessible to regular KPFM. It is worth nothing that the HV-KPFM technique has lower sensitivity than conventional KPFM limited by the amplification of the bias signal supplied to the tip by the input/output of the controller as well as the discretization of the bias signal by the controller before its amplification. For measuring surface potential in the ±10 V regime, we believe that conventional KPFM still offers the most effective platform. It is outside this potential regime that the developed HV-KPFM technique comes into its own and allows measurements that simply cannot be done otherwise. Finally, we have proposed a novel method for the measurement (and spatial mapping) of pyroelectric coefficients in ferroelectric single crystals, by using HV-KPFM to measure the generated pyroelectric voltage on heating and cooling. We believe the extension of surface potential measurement by KPFM to the high voltage regime will greatly expand the range of material processes accessible by KPFM, unlocking a new world of spatially resolved high voltage surface phenomena.

4. Experimental Section

Sample Preparation: The sample used in PTCR mapping composed of $BaTiO_3$–$PbTiO_3$–$CaTiO_3$ (BTO-PTO-CTO) where the percentage concentrations were 68%, 20%, and 12% respectively, with an average measured grain size diameter of 4 μm. The ceramics typically had relatively low bulk resistivity at room temperature (10–100 Ωcm). Samples for this study were prepared from bulk by cutting and polishing using diamond paper and a colloidal silica solution. Gold electrodes were deposited with an interelectrode gap of ≈40 μm via sputtering and KPFM was undertaken in the gap. For the pyroelectric measurements, a z-cut lithium niobate single crystal (obtained from MTI corporation, USA) was polished to the desired thickness.

Tip-Based Electrode Milling: For the investigations in Figure 2, an interelectrode gap was machined into a deposited gold electrode, by AFM micromachining. A silicon AFM tip with a cantilever of stiffness constant

of 40 Nm^{-1} was scanned over the metallic bar in contact mode. A large deflection set-point was used, which resulted in an enhanced compressive force (of ≈1 μN) being imparted from the tip to the sample. This resulted in the line-by-line removal the metallic film as the AFM tip scans. The scan window was positioned to generate an ≈50 μm gap in the deposited metallic bar.

Kelvin Probe Force Microscopy: For conventional KPFM studies, an Asylum Research MFP-3D Infinity Atomic Force Microscope was used in the amplitude-modulated KPFM mode to perform spatially resolved surface potential mapping in two-pass mode. For such measurements, a Pt-coated Si tip (Nanosensor PPP-EFM) with a stiffness constant of 2.8 Nm^{-1} was used (typical resonance frequency ≈70 kHz). The HV module was used with the same tips for the high voltage KPFM measurements. For KPFM measurements, the Pt-coated tip was calibrated using a Au-Al Budget Sensors KPFM and EFM sample to determine the work function of the tip before making potential measurements with the tip. The calibration procedure was also repeated for HV-KPFM measurements.

Heating the Pyroelectric Crystal: For the pyroelectric measurements, the sample was mounted on a sapphire substrate, which in turn was then mounted on a temperature-controlled ceramic heater. A platinum resistance temperature detector (Pt100-RTD) was used to allow the temperature to be measured and accurately controlled within 0.1 K via a Thor Labs TC200 temperature controller.

Supporting Information

Supporting Information is available from the Wiley Online Library or from the author.

Acknowledgements

C.J.M. and N.S. contributed equally to the work. A.K. and K.H. gratefully acknowledge support from the Department of Education and Learning NI through grant USI-205 and the Engineering and Physical Sciences Research Council via grant EP/S037179/1. J.M.G is grateful for the financial support received from the Engineering and Physical Sciences Research Council (EPSRC through grant EP/P02453X/1 and through studentship funding). R.G.P.M. gratefully acknowledges support via the UKRI Future Leaders Fellowship program (MR/T043172/1). The authors gratefully acknowledge the financial support received from Tezpur University, India in the form of Ph.D. studentship to NS under the collaborative TU-QUB PhD program. B.J.R. gratefully acknowledges support from the Science Foundation Ireland via SFI/21/UUS/3765.

Conflict of Interest

The authors declare no conflict of interest.

Data Availability Statement

The data that support the findings of this study are available from the corresponding author upon reasonable request.

Keywords

ferroelectrics, high-voltage KPFM, potential mapping, pyroelectrics, triboelectric

Received: February 1, 2024
Revised: March 16, 2024
Published online: April 5, 2024

[1] M. Nonnenmacher, M. P. Oboyle, H. K. Wickramasinghe, *Appl. Phys. Lett.* **1991**, *58*, 2921.
[2] W. Melitz, J. Shen, A. C. Kummel, S. Lee, *Surf. Sci. Rep.* **2011**, *66*, 1.
[3] T. Glatzel, S. Sadewasser, R. Shikler, Y. Rosenwaks, M. C. Lux-Steiner, *J. Mater. Sci. Eng. B* **2003**, *102*, 138.
[4] R. Giridharagopal, J. T. Precht, s. Jariwala, L. Collins, S. Jesse, S. V. Kalinin, D. S. Ginger, *ACS Nano* **2019**, *13*, 2812.
[5] N. Balke, P. Maksymovych, S. Jesse, I. I. Kravchenko, Q. Li, S. V. Kalinin, *ACS Nano* **2014**, *8*, 10229.
[6] M. J. Shearer, M. Y. Li, L. J. Li, S. Jin, R. J. Hamers, *J. Phys. Chem. C* **2018**, *122*, 13564.
[7] W. Yim, V. Nguyen, Q. T. Phung, H. S. Kim, Y. H. Ahn, S. Lee, J. Y. Park, *ACS Appl. Mater. Interfaces* **2022**, *14*, 26295.
[8] V. Panchal, R. Pearce, R. Yakimova, A. Tzalenchuk, O. Kazakova, *Sci. Rep.* **2013**, *3*, 2597.
[9] P. Biglarbeigi, A. Morelli, S. Pauly, Z. D. Yu, J. Jiang, S. Sharma, D. Finlay, A. Kumar, N. Soin, A. F. Payam, *ACS Nano* **2023**, *17*, 21506.
[10] J. R. Maguire, H. Waseem, R. G. P. McQuaid, A. Kumar, J. M. Gregg, C. Cochard, *Adv. Electron. Mater.* **2022**, *8*, 2101384.
[11] M. P. Campbell, J. P. V. McConville, R. G. P. McQuaid, D. Prabhakaran, A. Kumar, J. M. Gregg, *Nat. Comm.* **2016**, *7*, 13764.
[12] S. W. Schmitt, R. K. Vasudevan, M. Seifert, A. Y. Borisevich, V. Deshpande, S. V. Kalinin, C. Dubourdieu, *ACS Appl. Electron Mater.* **2021**, *3*, 4409.
[13] M. Ziatdinov, D. Kim, S. Neumayer, L. Collins, M. Ahmadi, R. K. Vasudevan, S. Jesse, M. H. Ann, J. H. Kim, S. Kalinin, *J. Appl. Phys.* **2020**, *128*, 055101.
[14] G. de Tournadre, F. Reisdorffer, R. Rodel, O. Simonetti, H. Klauk, L. Giraudet, *J. Appl. Phys.* **2016**, *119*, 125501.
[15] D. S. Jakob, N. Li, H. Zhou, X. G. Xu, *Small* **2021**, *17*, 2102495.
[16] M. Lee, W. Lee, F. B. Prinz, *Nanotechnology* **2006**, *17*, 3728.
[17] S. Barbet, M. Popoff, H. Diesinger, D. Deresmes, D. Théron, T. Mélin, *J. Appl. Phys.* **2014**, *115*, 144313.
[18] J. J. Steffes, R. A. Ristau, R. Ramesh, B. D. Huey, *Proc. Natl. Acad. Sci. U S A.* **2019**, *116*, 2413.
[19] Y. Tikhonov, J. R. Maguire, C. J. McCluskey, J. P. V. McConville, A. Kumar, H. D. Lu, D. Meier, A. Razumnaya, J. M. Gregg, A. Gruverman, V. M. Vinokur, I. Luk'yanchuk, *Adv. Mater.* **2022**, *34*, 2203028.
[20] K. M. Holsgrove, D. M. Kepaptsoglou, A. M. Douglas, Q. M. Ramasse, E. Prestat, S. J. Haigh, M. B. Ward, A. Kumar, J. M. Gregg, M. A. Arredondo *APL Mater.* **2017**, *5*, 066105.
[21] P. W. Turner, J. P. V. McConville, S. J. McCaftan, M. H. Campbell, J. Schaab, R. G. P. McQuaid, A. Kumar, J. M. Gregg, *Nano Lett.*.**2018**, *18*, 6381.
[22] J. R. Maguire, C. J. McCluskey, K. M. Holsgrove, A. Suna, A. Kumar, R. G. P. McQuaid, J. M. Gregg, *Nano Lett.* **2023**, *23*, 10360.
[23] R. D. Roseman, N. Mukherjee, *J. Electroceram.* **2003**, *10*, 117.
[24] A. F. Diaz, R. M. Felix-Navarro, *J. Electrostat.* **2004**, *62*, 277.
[25] O. Prakash, S. Tiwari, P. Maiti, *ACS Omega* **2022**, *7*, 34718.
[26] P. F. Zhao, N. Soin, A. Kumar, L. Shi, S. L. Guan, C. Tsonos, Z. D. Yu, S. C. Ray, J. A. McLaughlin, Z. G. Zhu, E. P. Zhou, J. F. Geng, C. H. See, J. K. Luo, *Nano Energy* **2020**, *67*, 104291.
[27] P. F. Zhao, N. Soin, K. Prashanthi, J. K. Chen, S. R. Dong, E. P. Zhou, Z. G. Zhu, A. A. Narasimulu, C. D. Montemagno, L. Y. Yu, J. K. Luo, *ACS Appl. Mater. Interfaces*. **2018**, *10*, 5880.
[28] F. Pertl, J. C. Sobarzo, L. Shafeek, T. Cramer, S. Waitukaitis, *Phys. Rev. Mater.* **2022**, *6*, 125605.
[29] D. Damjanovic, *Rep. Prog. Phys.* **1998**, *61*, 1267.

[30] J. Groten, M. Zirkl, G. Jakopic, A. Leitner, B. Stadlober, *Phys. Rev. B* **2010**, *82*, 054112.
[31] A. Savage, *J. Appl. Phys.* **1966**, *37*, 3071.
[32] R. S. Weis, T. K. Gaylord, *Appl. Phys. A* **1985**, *37*, 191.
[33] R. E. Newnham, *Structure-Property Relations*, Springer, NY, USA **2012**.
[34] T. Bartholomaus, K. Buse, C. Deuper, E. Kratzig, *Phys. Status Solidi A* **1994**, *142*, K55.